Journal of Applied Research in Water and Wastewater
E-ISSN: 2476-6283
Journal homepage: https://arww.razi.ac.ir

Green synthesis of Cu-doped TiO_2 nanoparticles via Cannabis Sativa Leaves for efficient adsorption of cationic dyes from wastewater

Seyed Mehdi Sajjadi*, Ghader Hosseinzadeh

Department of Chemical Engineering, Faculty of Interdisciplinary Sciences and Technologies, University of Bonab, Bonab, Iran.

GRAPHICAL ABSTRACT

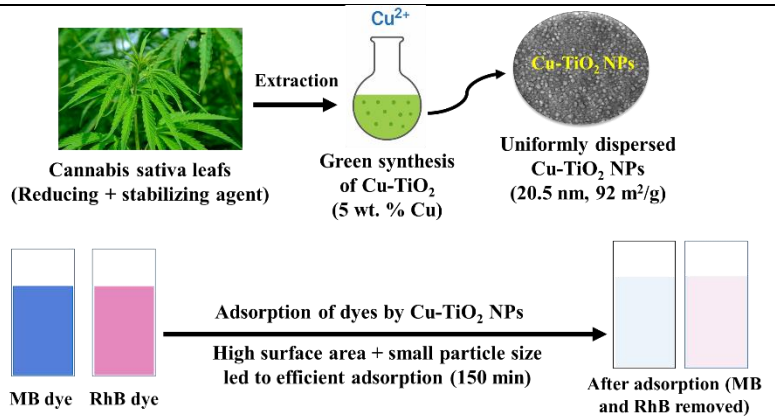

ARTICLE INFO

Article type:
Research Article

Article history:
Received 12 June 2025
Reviewed 20 September 2025
Received in revised form 24 September 2025
Accepted 30 December 2025

Keywords:
Cu-doped TiO_2
Green synthesis
Cannabis Sativa
Cationic dyes adsorption
Wastewater treatment

ABSTRACT

In this study, 5 wt. %Cu-doped TiO_2 nanoparticles (NPs) were synthesized through a green and sustainable method, utilizing Cannabis sativa leaf extract as a reducing agent to promote eco-friendly wastewater treatment. The NPs were characterized using XRD, FESEM, BET, EDAX, and TEM, revealing uniform dispersion, an average particle size of approximately 20.5 nm, and a high surface area of 92 m²/g. These NPs were employed for adsorption of Methylene Blue (MB) and Rhodamine B (RhB) dyes from aqueous solutions at initial concentrations of 1–10 mg/L. Adsorption experiments, conducted over 150 min, showed equilibrium data best fitting the Freundlich isotherm (R^2 = 0.9979 for MB, 0.9995 for RhB), indicating multilayer adsorption. Kinetic studies confirmed that the Elovich models provided the best fit (R^2 > 0.997), suggesting chemisorption-dominated processes. The NPs exhibited high adsorption efficiency, offering a cost-effective and sustainable solution for treating textile wastewater, addressing critical environmental challenges posed by industrial dyes.

1. Introduction

The rapid expansion of industries such as textiles, leather, paper, and pharmaceuticals has increased environmental pollutants, particularly textile dyes, which pose significant risks to human health and water resources (Bopape *et al.,* 2024; Sajjadi *et al.,* 2025a). Dyes such as Methylene Blue (MB) and Rhodamine B (RhB) in textile wastewater exacerbate water scarcity by contaminating rivers and lakes (Nawaz *et al.,* 2023; Sajjadi *et al.,* 2025b; Munyegaju *et al.,* 2022). These dyes are toxic, non-biodegradable, and resistant to conventional treatment methods, and their presence in water can reduce light penetration, inhibit photosynthesis in aquatic ecosystems, and can cause severe health problems such as skin irritation, respiratory issues, and even carcinogenic effects (Sharma *et al.,* 2022; Dutta *et al.,* 2024). These pollutants requirer effective removal methods, as traditional biological, chemical, and physical techniques often fail due to incomplete degradation or secondary pollutant generation (Piaskowski *et al.,* 2019; Hosseinzadeh *et al.,* 2024).

Nanomaterials, with their high surface area, chemical stability, and eco-friendly properties, have emerged as promising alternatives methods (Khin *et al.,* 2012; Sajjadi *et al.,* 2022b; Sajjadi *et al.,* 2022a). Materials such as carbon nanotubes, graphene derivatives, and nanocomposites demonstrate excellent dye adsorption capacities (Ahlawat *et al.,* 2020; Baratta *et al.,* 2025; Sadeghpour *et al.,* 2022), offering innovative and cost-effective solutions compared to conventional methods (Sajjadi *et al.,* 2024a). Among these, TiO_2 nanoparticles (NPs) are widely studied for their large surface area, surface charge, chemical stability, and photocatalytic activity, making them ideal for dye removal (Cheng *et al.,* 2014; MiarAlipour *et al.,* 2018; Sajjadi 2024). To enhance performance, TiO_2-based nanocomposites, combining TiO_2 with metals, metal oxides, or carbon-based materials, have been developed to improve adsorption efficiency and stability (Jaramillo-Fierro *et al.,* 2024). For instance, Fe-doping increases reactive sites for dye adsorption (Rahman et al., 2023), while Ag-doping enhances optical properties for visible-light-driven dye removal (Nagaraj *et al.,* 2021). Similarly, combining TiO_2 with carbon-based

*Corresponding author Email: seyedmehdi_sajjadi@yahoo.com
Mehdi_sajjadi@ubonab.ac.ir

How to cite: S.M. Sajjadi, G. Hosseinzadeh, Green synthesis of Cu-doped TiO_2 nanoparticles via Cannabis Sativa Leaves for efficient adsorption of cationic dyes from wastewater, *Journal of Applied Research in Water and Wastewater*, 12 (2), 2025, 157-166. doi: https://doi.org/10.22126/arww.2025.12327.1379

materials like graphene or carbon nanotubes boosts adsorption capacity due to their porous structure and high surface area (Kuvarega *et al.,* 2017). However, traditional synthesis methods often rely on costly or hazardous precursors, posing environmental and economic challenges (Sajjadi *et al.,* 2019). In contrast, green synthesis methods have emerged as eco-friendly alternatives, using natural plant extracts as reducing and capping agents to minimize environmental impact and lower production costs (Verma *et al.,* 2022; Eddy *et al.,* 2024; Al-Assaly *et al.,* 2024).

Various plant parts such as roots, leaves, fruits, peels, and flowers have been successfully utilized in the green synthesis of NPs, leveraging their rich bioactive compounds like polyphenols, flavonoids, and alkaloids that facilitate nanoparticle formation and stabilization (Ho *et al.,* 2025; Saini *et al.,* 2023; Yitagesu *et al.,* 2023). For example, TiO_2 NPs synthesized using Citrus limetta peel extract demonstrated a uniform spherical morphology with particle sizes ranging between 80 and 100 nm, where citric acid in the extract functioned as an effective reducing and capping agent (Nabi *et al.,* 2021). Similarly, Averrhoa bilimbi, a medicinal plant known for its phenolic, flavonoid, and tannin content, has been used successfully for TiO_2 NPs synthesis, yielding materials with excellent properties (Abisharani *et al.,* 2020).Baccaurea racemosa peel extract, rich in flavonoids, phenolic, and terpenoids, has also been utilized for green synthesis of TiO_2 NPs. The resulting anatase-phase TiO_2 exhibited high crystallinity, uniform spherical morphology (~32 nm), and excellent particle stability, attributed to the stabilizing effect of bioactive compounds. These NPs demonstrated high efficiency in removing of Acid Red-185 dye (Deliza *et al.,* 2025).

Moreover, Beta vulgaris (beetroot) peel extract, containing the bioactive pigment betanin, has been used as a reducing and stabilizing agent in the green synthesis of Ag/TiO_2 nanocomposites, producing spherical NPs with uniform size distribution. The synthesized materials showed high dye removal efficiency for MB, Congo red, and methyl orange dyes (BinSabt *et al.,* 2022). Achyranthes aspera leaf extract, rich in polyphenols and flavonoids, was also employed to synthesize $Ag@TiO_2$ nanomaterials with promising properties for dye removal applications (Jadhav *et al.,* 2025).Gadge and colleagues used Piper betel leaf extract to synthesize Gd/TiO_2 NPs, demonstrating their potential in wastewater treatment applications (Gadge *et al.,* 2025).

Cedrus deodara leaf extract has been applied for green synthesis of $Cu@TiO_2$ nanocomposites, yielding uniform NPs with enhanced surface properties due to the plant's high phenolic content. The small particle size (~10 nm) and increased surface area resulted in strong adsorption capacity for dye removal, with high efficiency observed for MB degradation (Ramzan *et al.,* 2021).

Cannabis sativa (CS) leaf extract, which is rich in phenolic compounds, flavonoids, and polysaccharides, has been effectively utilized to prevent NPs agglomeration through strong interactions involving hydroxyl groups present in these biomolecules. Due to these properties, CS extracts have been successfully employed in the green synthesis of various NPs, including silver and bimetallic gold-silver NPs (Csakvari *et al.,* 2021; Abbasi *et al.,* 2018). Additionally, the leaf extract of CS has been used to synthesize TiO_2 NPs characterized by uniform particle distribution and small size (~12.5 nm), which demonstrated high efficiency in removing MB dye from aqueous solutions, thereby confirming their potential for eco-friendly and sustainable dye remediation applications (Jayapriya *et al.,* 2021). In another study, calcium-doped TiO_2 NPs synthesized using CS leaf extract exhibited superior physicochemical characterization and showed excellent performance in the removal of textile dyes from wastewater (Sajjadi *et al.,* 2025c).

In summary, green synthesis of NPs using various plant extracts has gained considerable attention recently due to its environmental friendliness, cost-effectiveness, and simplicity. To the best of our knowledge, Cu-doped TiO_2 NPs have not yet been synthesized using a green method based on CS leaf extract. Therefore, this study employs an eco-friendly and sustainable synthesis route for Cu-doped TiO_2 NPs using CS leaves, eliminating the need for toxic chemicals and high energy consumption. The synthesized nanomaterials were evaluated for their dye removal efficiency across different concentrations, and their adsorption behaviour was systematically investigated using various isotherm and kinetic models for MB and RhB removal. This study introduces a novel green synthesis method for Cu-TiO_2 NPS and provides comprehensive insight into their adsorption performance under various operational conditions.

2. Materials and methods

2.1 Materials

In the NPs preparation process, titanium (IV) isopropoxide (TTIP, $Ti[OCH(CH_3)_2]_4$, CAS No. 546-68-9) and copper (II) nitrate trihydrate ($Cu(NO_3)_2{\cdot}3H_2O$, CAS No. 10031-43-3) were used as titanium and copper precursors, respectively. Both chemicals were purchased from Merck with analytical grade purity. RhB and MB, obtained from Merck, were selected as model organic dye contaminants, with their properties detailed in Table 1. Deionized (DI) water served as the solvent throughout the procedure. Additionally, CS leaves were gathered from the East Azerbaijan region for use in this study.

Table 1. Physicochemical properties of MB and RhB.

Dye name	Dye type	Chemical Formula	Molecular weight, g/mol	Solubility in Water, mg/mL	λ_{max}, nm
MB	Cationic	$C_{16}H_{18}ClN_3S$	319.85	43.6	665
RhB	Cationic	$C_{16}H_{18}ClN_2O_3$	479.02	50	552

2.2. NPs preparation and procedures

A green synthesis route was employed to prepare Cu-doped TiO_2 NPs using a natural plant extract as both a reducing and a stabilizing agent. Initially, Cannabis sativa leaves were collected, washed thoroughly with distilled water to remove surface impurities, and then air-dried. The dried leaves were finely chopped and heated in deionized water at 60 °C for 1 h to prepare the extract. The extract obtained from Cannabis sativa leaves was prepared by aqueous extraction and subsequent centrifugation. This light brown solution is referred to as ECSL, which stands for Extract from Cannabis Sativa Leaves. ECSL acts as a natural reducing and stabilizing agent in the green synthesis process.

For the synthesis of NPs, 7.04 mL of TTIP was stirred in 50 mL of DI water at 60 °C for 1 h to form a homogeneous solution. Then, 10 mL of ECSL was added dropwise to the TTIP solution while maintaining stirring for an additional 2h. Separately, 0.38 g of $Cu(NO_3)_2{\cdot}3H_2O$ was dissolved in DI water and incorporated into TTIP-ECSL mixture. Following this, an additional 5 mL of ECSL was gradually added to solution, which was then stirred for an extra 2 h before being allowed to cool. The mixture was centrifuged at 4000 rpm for 15 min, and the solid precipitate was collected. The precipitate was washed twice with DI water to remove impurities, dried at 110 °C for 12 h, and then calcined at 600 °C for 5 h. The final product was a green-synthesized 5 wt. % Cu-doped TiO_2 NPs.

In this study, 5 wt.% Cu-doped TiO_2 NPs were synthesized. The choice of 5 wt.% Cu loading was guided by previous research indicating that this level is typically sufficient to enhance surface area, improve particle dispersion, and reduce particle size without triggering the formation of undesirable copper-based secondary phases. Generally, Cu loadings above 5 wt.% tend to result in unsuccessful doping, leading to aggregation or the formation of separate phases, which may compromise structural uniformity and surface properties. Cu additions below this threshold, typically less than 5 wt. %, were reported to positively influence structural characteristics and, ultimately, enhance the performance of the NPs (Adamu *et al.,* 2023; Khan *et al.,* 2022; Aguilar *et al.,* 2013; Sajjadi *et al.,* 2025b; Natsir *et al.,* 2021). Thus, 5 wt. % was chosen to maintain a balance between high adsorption capacity and structural stability.

2.3. Nanoparticles characterization

The crystalline structure of the NPs was analyzed using X-ray diffraction (XRD) patterns obtained with a Philips X'Pert MPD diffractometer (Philips, Netherlands), equipped with Cu Kα radiation (λ = 0.15406 nm). The measurements were carried out in the 2θ =20–80°. The surface morphology and elemental composition of NPs were examined using field-emission scanning electron microscopy (FESEM) and energy-dispersive X-ray spectroscopy (EDAX), both performed with a MIRA3 TESCAN instrument (TESCAN, Czech Republic). Furthermore, both particle size distribution and 3D surface morphology were quantitatively analyzed from the FESEM images using ImageJ software. These techniques provided insights into the shape, size distribution, and elemental mapping of the synthesized NPs. To obtain further information about the internal structure and particle size at the nanoscale, transmission electron microscopy (TEM) was conducted using a Leo 906 E microscope (ZEISS, Germany). Additionally, the specific surface area of NPs was determined via BET analysis using a Quantachrome ChemBET-3000 instrument (Quantachrome Instruments, USA).

2.4 Adsorption experiments

2.4.1 Analytical methods

To evaluate the adsorption performance of the synthesized NPs, aqueous solutions of MB and RhB were prepared at various concentrations (1, 3, 5, 7, and 10 mg/L). In each test, 0.1 g of the adsorbents was dispersed in 100 mL of dye solution and continuously

mixed using a magnetic stirrer at 200 rpm to ensure uniform dispersion. At regular intervals of 30 min, 4 mL of the suspension was withdrawn and immediately centrifuged to separate the suspended particles. The absorbance of the resulting clear supernatant was measured using a SHIMADZU UV–1800 spectrophotometer (Shimadzu, Japan) at 665 nm for MB and 552 nm for RhB. Each measurement was repeated three times to confirm reproducibility. All adsorption experiments were performed at a constant temperature of 25 °C to ensure consistency. The dye removal efficiency (R, (%)) was calculated according to the following equation.

$$R(\%) = \left(1 - \frac{C_t}{C_0}\right) \times 100 \quad (1)$$

C_0 (mg/L) represents the initial dye concentration. Also, C_t (mg/L) denotes the dye concentration at a specific time t after adsorption.

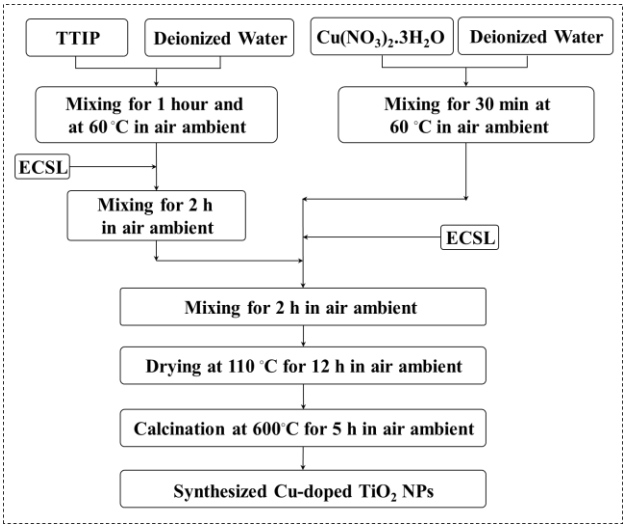

Fig. 1. Synthesis diagram of the Cu-doped TiO_2 NPs.

Moreover, the adsorption capacity (q_e) and amount of adsorption at different times (q_t) were calculated by the Eqs. 2 and 3, respectively.

$$q_e = (C_0 - C_e) \times \left(\frac{V}{m}\right) \quad (2)$$

$$q_t = (C_0 - C_t) \times \left(\frac{V}{m}\right) \quad (3)$$

In mentioned equations, V was the volume of solution (L), and m is the mass of NPs (g). Also, unit of both q_e and q_t was (mg/g).

2.4.2. Applied adsorption isotherms

Next, the relationship between dye adsorption and initial concentration of dye is discussed through isotherm modelling. These relationships are commonly described by mathematical models such as the Langmuir, Freundlich, and Temkin isotherms. In this section, the corresponding equations and a brief explanation of each isotherm are presented. The comparison of these models and identification of the most accurate one based on error analysis were addressed in the Results and Discussion section.

2.4.2.1. Langmuir isotherm

The isotherm of Langmuir derives from the balance within adsorption and desorption steps. According to the fundamentals of this isotherm, adsorption proceeds on a uniform surface. The adsorption energy remains uniform across all sites. Furthermore, when a dye molecule binds to a specific site, further adsorption at that location is precluded. Langmuir isotherm is matched by Henry equation for dilute concentrations (Osmari *et al.,* 2013). This model presupposes monolayer coverage of the adsorption surface and is applicable for a smaller amount of the adsorbent. The discussed model was exhibited in Eq. 4 (Dada *et al.,* 2012).

$$q_e = \left(\frac{q_m K_L C_e}{1 + K_L C_e}\right) \quad (4)$$

In the above noted equation q_e indicates amount of substance absorbed per gram of adsorbent (mg/g). Also, q_m indicates the highest adsorption capacity for adsorbent (mg/g). Moreover, K_L is the Langmuir constant (L.mol^{-1}). Various linear representations of the Langmuir model have been documented in the published works (Osmari *et al.,* 2013; Chiani *et al.,* 2020). Langmuir isotherm type 1, 2 and 3 were presented in Eqs. 5- 7, respectively.

$$\frac{C_e}{q_e} = \frac{1}{q_m K_L} + \frac{C_e}{q_m} \quad (5)$$

$$\frac{1}{q_e} = \frac{1}{q_m} + \left(\frac{1}{q_m K_L}\frac{1}{C_e}\right) \quad (6)$$

$$q_e = q_m - \frac{1}{K_L}\frac{q_e}{C_e} \quad (7)$$

It must be noted, q_m and K_L for every type will be obtained from the drawing and investigation of the above mentioned equations (Osmari *et al.,* 2013). The adsorption behaviour of MB and RhB will be evaluated by constructing plots of C_e/q_e vs C_e, $1/q_e$ vs $1/C_e$ and q_e vs q_e/C_e, representing Langmuir types I, II, and III, respectively. Moreover, as demonstrated in recent studies, the dimensionless separation factor (R_L) derived from the Langmuir equation can effectively indicate the favourability of the adsorption process. Values of $0 < R_L < 1$ reflect favorable adsorption. $R_L > 1$ shows unfavorable adsorption. R_L was obtained from Eq. 8.

$$R_L = \frac{1}{1 + K_L C_0} \quad (8)$$

where, K_L (L mol^{-1}) and C_0 (mol L^{-1}) are the Langmuir constant and initial concentration of dye, respectively (Habeeb *et al.,* 2023).

2.4.2.2. Freundlich isotherm

Owing to the literature, Freundlich isotherm was the first adsorption equation that was presented. Moreover, generally, Freundlich isotherm was applied as a model for describing the adsorption in heterogeneous surfaces. In examination of adsorption using the Freundlich model, it is important to recognize that Henry's law is not applicable for dilute concentrations. Furthermore, this model is suitable for multilayer adsorption (Dada *et al.,* 2012). The Freundlich adsorption model is given by:

$$q_e = K_F C_e^{\left(\frac{1}{n}\right)} \quad (9)$$

The linear form of Freundlich isotherm which used in our calculations is described as:

$$\ln(q_e) = \ln(K_F) + \frac{1}{n}(\ln C_e) \quad (10)$$

Constants of Freundlich isotherm are K_F and n^{-1}. K_F presents the adsorption capacity. Also, n^{-1} is a function of adsorption strength. Value of n^{-1} shows the type of isotherm to be irreversible ($n^{-1} = 0$), typical adsorption ($0 < n^{-1} < 1$), and unfavourable ($n^{-1} > 1$) (Osmari *et al.,* 2013; Dada *et al.,* 2012). Furthermore, the maximum adsorption capacity (q_m) was also estimated based on the Freundlich isotherm model using the equation $q_m = K_F C_0^{1/n}$ (Nayebzadeh *et al.,* 2021; Rahmanivahid *et al.,* 2020).

2.4.2.3. Temkin isotherm

The Temkin model incorporates a variable that explicitly accounts for the interactions among the adsorbent and the adsorbate. Concerning the Temkin model, an increase in the covering rate of adsorbent surface results in a decrease in the adsorption heat of molecules (Osmari *et al.,* 2013; Chu 2021; Dada *et al.,* 2012). Moreover, Temkin isotherm (Eq. 11) studies the influence of temperature on adsorption, which decreases proportionally with the extent of adsorbate and adsorbent.

$$q_e = \frac{RT}{b}\ln(K_T) + \frac{RT}{b}(\ln C_e) \quad (11)$$

K_T is the equilibrium binding constant (L/mol). Also, b is Temkin model constant and corresponds to the adsorption heat. R is the universal gas constant and T is temperature (K). In addition, RT/b is slope and ((RT/b)*ln KT) is intercept.

2.4.3. Applied adsorption kinetics

To investigate the possible adsorption mechanism, various kinetic models, including pseudo-first-order, pseudo-second-order, intra-

particle diffusion, and Elovich models, were applied for evaluation of dye removal by Cu-doped TiO_2 NPs.
The descriptions and corresponding equations of the mentioned kinetic models are provided below. These models were analyzed and discussed in detail in the results and discussion section.

2.4.3.1. Pseudo first order model

Aim of this study was focused on the dyes adsorption in aqueous solution. Based on the literature, the pseudo first order model is one of the most applied models in cited situations. By starting from the Lagergren equation and some mathematical simplifications, the final state of pseudo first order model (Eq. 12) was obtained.

$$\ln(q_e - q_t) = \ln(q_e) - k_1 t \quad (12)$$

In Eq. 12, q_e and q_t were the amount of adsorbed dyes (mg/g) at equilibrium and time t (min), correspondingly. Also, k_1 was the rate constant (min^{-1}) (Revellame *et al.,* 2020).

2.4.3.2. Pseudo second order model

Pseudo second order model is another conventional kinetics model which was used in the evaluation of the adsorption processes. In this model, as presented in Eq. 13, graph of the reverse amount of the adsorbed dye in various times versus reverse time was drawn. The slops and intercept of the plot indicated the qe and k_2, respectively (Ahmad *et al.,* 2023).

$$\frac{1}{q_t} = \left(\frac{1}{k_2 {q_e}^2}\right)\frac{1}{t} + \frac{1}{q_e} \quad (13)$$

2.4.3.3. Elovich model

Another model which was tested for dyes adsorption was Elovich model. This model suggest that the rate of dyes adsorption descends exponentially as the quantity of adsorbed dye ascends. The Elovich model was illustrated as follow:

$$\frac{dq_t}{dt} = \alpha e^{-\beta q t} \quad (14)$$

For solving the mentioned equation, boundary condition is required which are as follow: q_t=0 at t=0 and $q_t = q_t$ at t=t. By considering the boundary condition and some mathematical simplifications, the final state of Elovich model (Eq. 15) was obtained.

$$q_t = \frac{1}{\beta}\ln(\alpha\beta) + \frac{1}{\beta}\ln(t) \quad (15)$$

In Eq. 15, α is the initial sorption rate (mg/g.min). Also, β is extend of surface coverage (g/mg). The slops and intercept of q_t vs t plot, indicated the $\frac{1}{\beta}$ and $\frac{1}{\beta}\ln(\alpha\beta)$, respectively (Cheung *et al.,* 2000).

2.4.3.4. Intra-particle diffusion model

The last model which was evaluated was Intra-particle diffusion model which assumes that the internal diffusion of the adsorbate was the rate determining step. This model was described with Eq. 16.

$$q_t = k_i t^{0.5} + C \quad (16)$$

where, k_i was the rate constant ($mg/g.min^{0.5}$) and C (mg/g) was boundary layer diffusion effects (An 2020).

3. Results and discussion

3.1 NPs characterization

3.1.1 XRD characterization

XRD patterns of NPs were recorded in the 2θ range of 20–80° and shown in Fig. 2. Peaks at 25.33, 36.01, 37.90, 48.06, 53.96, 55.06, 62.70, 69.01, 70.41, and 75.32° were detected, corresponding to the planes (101), (103), (004), (200), (105), (211), (204), (116), (220), and (215). A comparison of these peaks with literature data confirmed that the formed structure is attributed to the anatase phase of TiO_2, as verified by matching the results with JCPDS card No. 84-1285 (Ahmad *et al.,* 2021). Fig. 2 also presents the XRD patterns of both pure TiO_2 and Cu-doped TiO_2 NPs for comparison. No additional peaks related to metallic copper or copper oxide phases (such as CuO or Cu_2O) were detected in the doped sample, suggesting that Cu^{2+} ions were likely incorporated into the TiO_2 lattice without forming separate crystalline phases. However, due to the absence of distinct copper peaks, the actual presence of Cu must be confirmed by elemental analysis, which will be addressed in the EDAX section. In addition, a comparison of the two XRD patterns reveals that the diffraction peaks of the Cu-doped TiO_2 are slightly less intense and broader than those of pure TiO_2. This broadening and intensity reduction are indicative of a decrease in crystallite size and improved dispersion of particles as a result of Cu doping. To verify this, crystallite sizes were calculated using X'Pert HighScore Plus software along with the Scherrer equation. The estimated crystallite size for pure TiO_2 was approximately 27.6 nm, while that of Cu-doped TiO_2 was 16.3 nm, confirming the significant reduction in crystallite size due to copper incorporation.

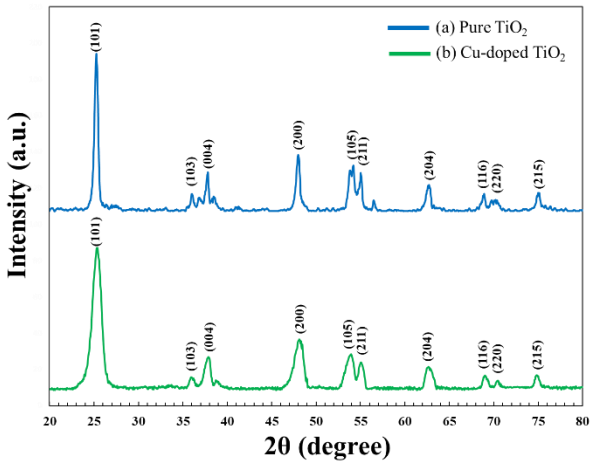

Fig. 2. XRD patterns: (a) Pure TiO_2 and (b) Cu-doped TiO_2

3.1.2. FESEM and BET characterization

FESEM image of NPs were displayed in Fig. 3a. The analysis revealed that the particles were uniformly dispersed, showed no signs of agglomeration, and had relatively similar sizes. A quantitative analysis of Fig. 3b using ImageJ software indicated that nearly all particles were smaller than 50 nm, with an average particle size of approximately 20.5 nm. These findings unequivocally confirm that the green-synthesized materials fall within the nanoscale and can be classified as NPs. Suitable dispersion of NPs might be ascribed to the green synthesis and employed CS.

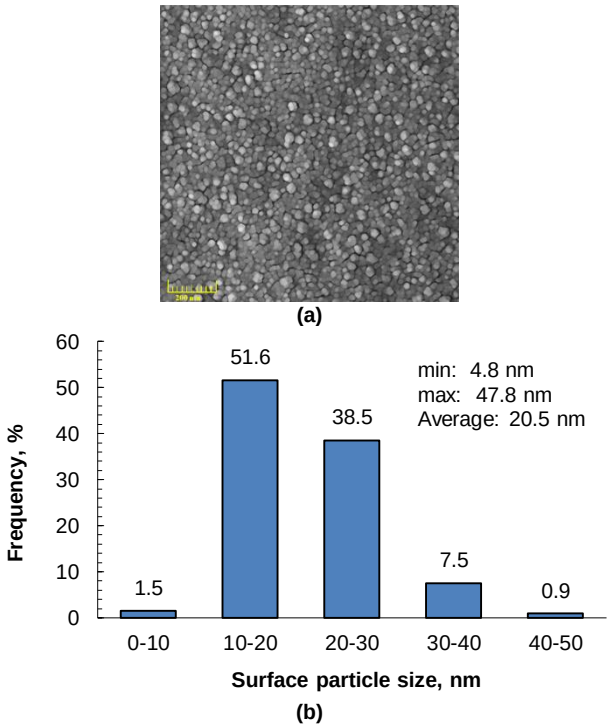

Fig. 3. (a) FESEM images of the Cu-doped TiO_2 NPs and (b) Particle size distribution.

It has been reported that the CS extract contains higher levels of phenolic, flavonoid, and polysaccharides. Cited components are

attached to the surface of NPs by applying OH groups and inhibit agglomeration. Noted trend led to the appropriate dispersion of NPs (Shahzadi *et al.,* 2022; Sajjadi *et al.,* 2024b; BinSabt *et al.,* 2022). Furthermore, BET characterization confirmed that the surface area of the NPs was 92 m^2/g. Due to their uniform dispersion and smaller particle size, the prepared NPs exhibit the potential for enhanced adsorption and dye removal efficiency, which will be evaluated in the next sections.

3D surface analysis of the synthesized NPs was exhibited in Fig. 4. The surface topography of NPs was compared via utilization of root mean square (RMS), maximum height (Hmax) and average height (Have). Topography images indicated that RMS, H_{max} and H_{ave} for fabricated NPs were 7.5, 52.9 and 22.9 nm, respectively. Generally, surfaces with appropriate roughness provide more active sites and enhance the interaction between adsorbate molecules and the adsorbent surface (Vieira *et al.,* 2018; Molla *et al.,* 2019).The relatively low surface roughness observed here suggests the presence of a large number of accessible active sites for dye adsorption. Thus, a high adsorption capacity is expected for the synthesized NPs, which will be further evaluated in the subsequent sections.

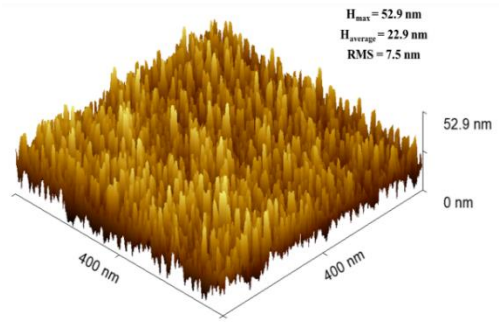

Fig. 4. Overview of 3D surface analysis of Cu-doped TiO_2 NPs

3.1.3. EDAX characterization

The findings from the EDAX characterization are presented in Fig. 5. As depicted in the images, all the constituent elements of the NPs were identified in the resulting structure. Thus, EDAX analysis verified the existence and dispersion of Ti, Cu and O in the structures of NPs. The quantitative elemental weight percentages are as follows: Cu: 4.2%, Ti: 60.5%, and O: 35.3%. Slight deviations may result from the localized nature of EDAX and its varying sensitivity to elements, such as underestimating light elements like oxygen and overestimating heavier ones like titanium. Thus, the absence of Cu-related peaks in the XRD pattern can be reasonably explained by the successful incorporation of Cu into the TiO_2 lattice, as further confirmed by EDAX analysis. Moreover, as shown in the images there was no significant agglomeration and the elements were homogeneously dispersed on the surface of adsorbent. These findings are consistent with the observations from XRD and FESEM analyses.

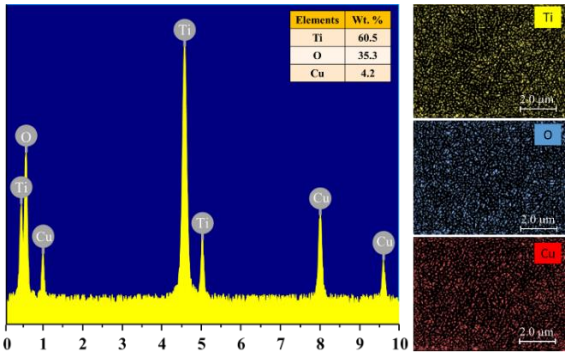

Fig. 5. EDAX analysis of the Cu-doped TiO_2 NPs.

3.1.4. TEM characterization

In order to further morphological investigation of the fabricated NPs, TEM analysis was performed. TEM image of NPs was depicted in Fig. 6. Generally, small metallic particles, uniform distribution of particles size and excellent dispersion can be evidenced for Cu-doped TiO_2 NPs. Fine and uniform metallic particles probably lead to the superior adsorption performance. Exhibited features are in line with FESEM and EDAX analysis.

3.2 Adsorption performance of NPs

3.2.1 Influence of initial concentration

It is obvious that Adsorption kinetic rate is dominated by mass transfer resistance. Initial concentration of dyes is the main driving force that is able to overcome the cited residence. Thus, influence of the dyes concentration is a key parameter in adsorption processes. Therefore, in this section effect of initial concentration in adsorption capacity and also, dyes adsorption was tested and results were displayed in Fig. 7. In this investigation different amounts of initial concentration (1, 3, 5, 7 and 10 mg/L) for MB and RhB were applied. Obtained data proved that, at first 60 min, graphs had steep slopes and the adsorption capacity rapidly raised. In the following, by increasing the adsorption time, slopes were reduced and after 150 min adsorption roughly was remained constant and reached to equilibrium condition. Generally, by increasing the initial concentration for both dyes, adsorption capacity was increased.

A comparison between MB and RhB adsorption shows that although their capacities were relatively close, RhB exhibited slightly higher adsorption capacity than MB under similar conditions. This may be attributed to the molecular structure and physicochemical properties of RhB. The larger molecular structure and higher hydrophobicity of RhB may enhance van der Waals forces and π–π stacking interactions between RhB and the surface of adsorbent. Moreover, the presence of additional functional groups (such as ethyl groups) in RhB may promote stronger interactions with the Cu-doped TiO_2 surface, resulting in more efficient adsorption (MiarAlipour *et al.,* 2018).

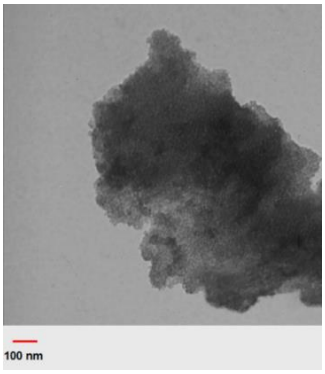

Fig. 6. TEM analysis of the Cu-doped TiO_2 NPs.

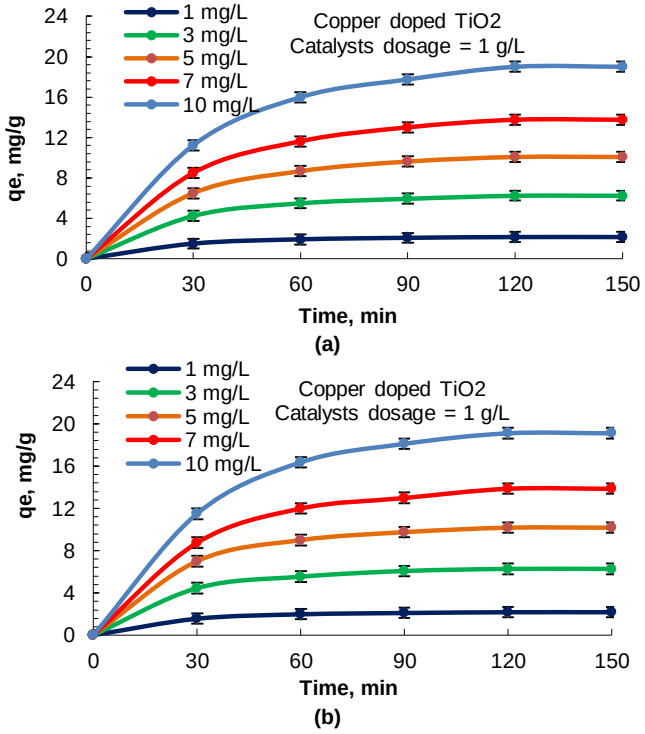

Fig. 7. Effect of dyes concentrations (a) MB and (b) RhB on the adsorption performance of NPs.

3.2.2. Adsorption isotherms

To better understand the adsorption mechanism, the evaluation of equilibrium data, commonly referred to as adsorption isotherms, is essential. These isotherms provide valuable insights into the interaction between dye molecules and the adsorbent surface, enabling both interpretation and prediction of the adsorption process. As previously described in section 2.4.2, three equilibrium models, Langmuir, Freundlich, and Temkin, were introduced.

In this section, the experimental equilibrium data obtained at 150 min for various initial dye concentrations (C_0) were analyzed using the aforementioned isotherm models. The goal is to identify the most appropriate model that best fits the experimental results. The fitting performance of each model is evaluated, and the results are compared and discussed in detail below.

3.2.2.1. Langmuir isotherms

Parameters of each type of Langmuir isotherms were extracted after curve fitting and obtained data were presented in Table 2. Based on the presented data in Table 2, R^2 for types 1, 2 and 3 for MB adsorption were 0.9916, 0.9799 and 0.9470, respectively. Also, R^2 for types 1, 2 and 3 for RhB adsorption were 0.9946, 0.9806 and 0.9177, respectively. Moreover, curve fitting graphs of dyes for the best type of Langmuir (type 1) were illustrated in Fig. 8. In addition, we can say that curve fitting for RhB was more compatible by experimental data in comparison with MB.

In addition, the separation factor (R_L) was calculated for all initial dye concentrations (C_0) for both dyes, and the results are summarized in Table 3. In all cases, the R_L values were found to be in the range of 0 to 1, indicating that the adsorption process is favorable according to the Langmuir isotherm. However, to identify the best-fitting isotherm overall, comparison of the R^2 values across all models remains essential.

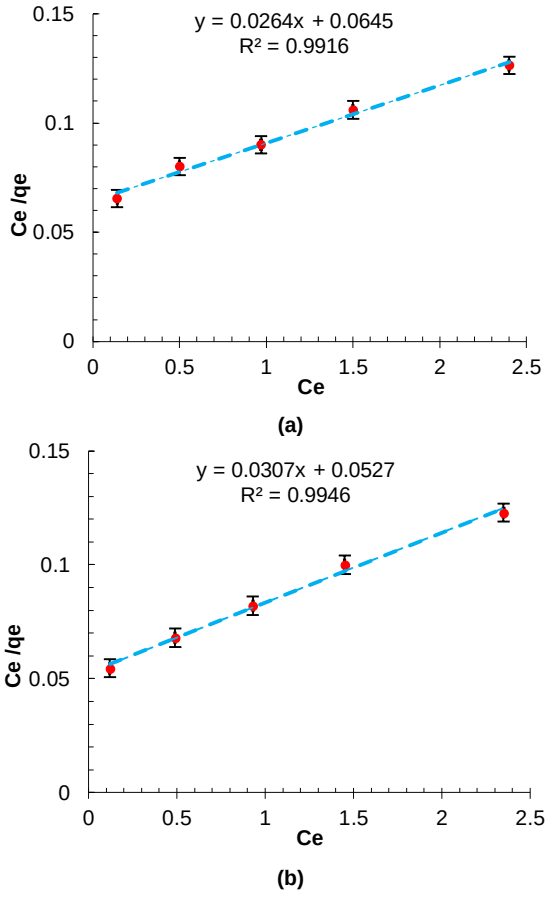

Fig. 8. Langmuir isotherms type 1 for adsorption of (a) MB and (b) RhB on Cu-doped TiO_2 NPs.

3.2.2.2. Freundlich isotherm

Validating of the obtained results by Freundlich model, for dyes adsorption via Cu-doped TiO_2 NPs was exhibited in Fig. 9. The constants, parameters, the maximum adoption capacity (q_m) for the Freundlich model and R^2 of isotherms were listed in Table 4. Based on the calculations, n^{-1} for MB and RhB were 0.7675 and 0.7713, respectively. Therefore, adsorption was normal and favorable. Moreover, R^2 of Freundlich isotherm for MB and RhB were 0.9979 and 0.9995, respectively. Moreover, the calculated q_m values were 59.04 mg/g for MB and 62.05 mg/g for RhB. In the study of adsorption isotherms for dyes on Cu-doped TiO_2, it was observed that Freundlich model offered a more accurate correlation compared to the Langmuir model.

Table 2. Parameters of Langmuir isotherms in dyes adsorption.

Isotherm	Parameters		
	q_m, mg/g	K_L, l/mg	R^2
Langmuir isotherm type 1 for MB adsorption	37.8787	0.409	0.9916
Langmuir isotherm type 2 for MB adsorption	21.2765	0.8818	0.9799
Langmuir isotherm type 3 for MB adsorption	34.1950	0.4620	0.9470
Langmuir isotherm type 1 for RhB adsorption	32.5732	0.5825	0.9946
Langmuir isotherm type 2 for RhB adsorption	18.2149	1.3009	0.9806
Langmuir isotherm type 3 for RhB adsorption	29.2220	0.6463	0.9177

Table 3. Parameters of Langmuir isotherms in dyes adsorption.

Initial concentration of MB (mg/L)	R_L for Langmuir type 1	R_L for Langmuir type 2	R_L for Langmuir type 3
1	0.7097	0.5314	0.6840
3	0.4490	0.2743	0.4191
5	0.3284	0.1849	0.3021
7	0.2589	0.1394	0.2362
10	0.1965	0.1018	0.1779
Initial concentration of RhB (mg/L)	**R_L for Langmuir type 1**	**R_L for Langmuir type 2**	**R_L for Langmuir type 3**
1	0.6319	0.4346	0.6074
3	0.3639	0.2040	0.3403
5	0.2556	0.1333	0.2363
7	0.1969	0.09895	0.1810
10	0.1465	0.07138	0.1339

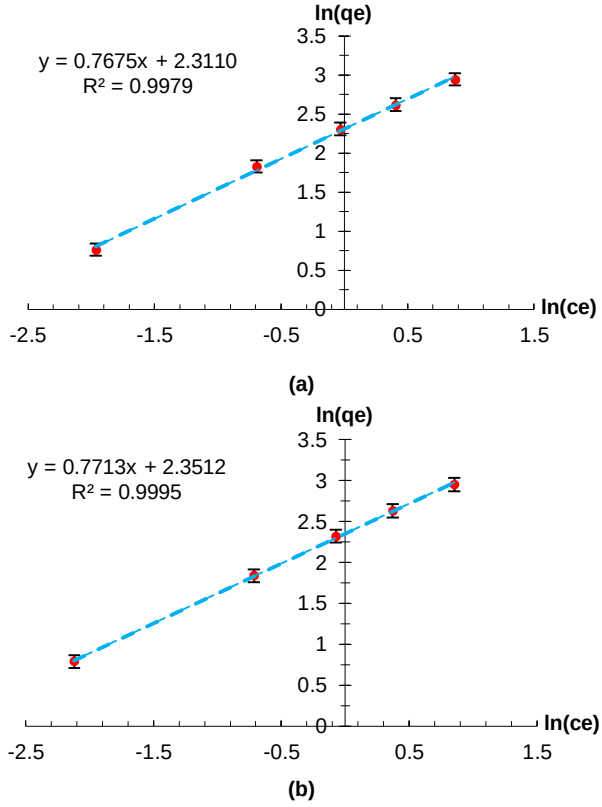

Fig. 9. Freundlich isotherm for adsorption of (a) MB and (b) RhB on Cu-doped TiO_2 NPs.

This can be attributed to the heterogeneous surface characteristics induced by Cu doping, which introduces adsorption sites with varying energy levels. Additionally, the synthesized NPs having an average size of approximately 20.5 nm and a specific surface area of around 92 m²/g, provide a wide range of active sites for adsorption. The diversity in

adsorption site energies corresponds well with the assumptions of the Freundlich model, thereby resulting in a better fit for describing the dye adsorption behaviour on these NPs.

3.2.2.3. Temkin isotherm

Obtained data for the dyes adsorption were compared with Temkin isotherm and results were presented in Fig. 10. Additionally, parameters of the Temkin isotherms are presented in Table 5. The temperature utilized in Temkin isotherm measurements was 298.15 K. Also, R^2 of Temkin isotherm for MB and RhB were 0.9273 and 0.9160, respectively.

Table 4. Parameters of Freundlich isotherm which was obtained from calculations.

Parameters / Isotherm	(1/n)	K_F, mg/g	q_m, mg/g	R^2
Freundlich isotherm for MB adsorption	0.7675	10.084	59.04	0.9979
Freundlich isotherm for RhB adsorption	0.7713	10.496	62.05	0.9995

Results revealed that R^2 of Temkin isotherm (for both dyes) were lower than the Freundlich isotherm and Langmuir isotherm type 1. Thus, it seems that Temkin model was not suitable isotherm in this case. Obtained trend was ascribed to the nature of Temkin isotherm. Temkin is appropriate for temperature-sensitive processes, whereas the temperature remained constant throughout this investigation. So, illustrated the lower compatibility in comparison with Langmuir and Freundlich isotherms.

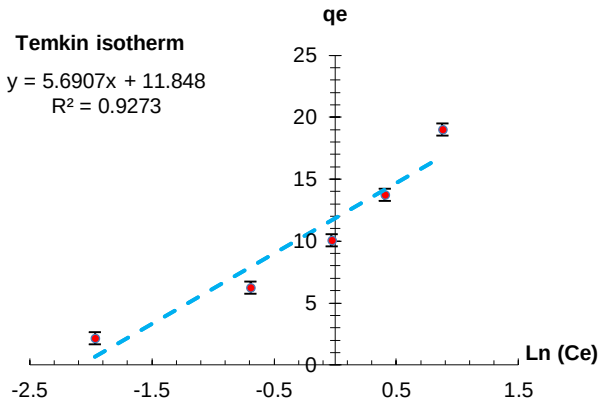

(a)

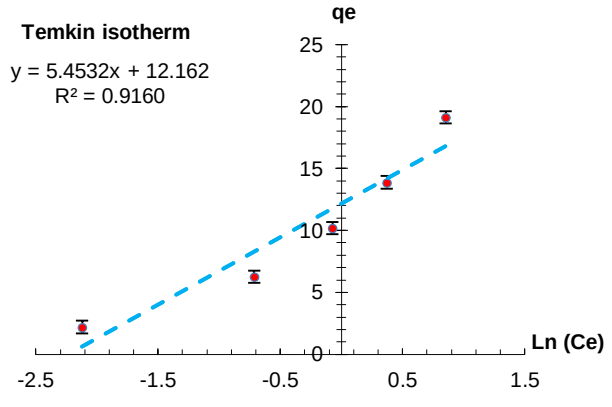

(b)

Fig. 10. Temkin isotherm for adsorption of (a) MB and (b) RhB on Cu-doped TiO_2 NPs.

Table 5. Parameters of Temkin isotherms in dyes adsorption.

Parameters / Isotherm	b, J.gr/mol^2	K_T, lit/mol	R^2
Temkin isotherm for MB adsorption	435.5912	8.0204	0.9273
Temkin isotherm for RhB adsorption	454.5622	9.3021	0.9160

According to the obtained results, the Freundlich isotherm exhibited excellent correlation with the experimental data for both MB (R^2 = 0.9979) and RhB (R^2 = 0.9995). This outcome can be attributed to the heterogeneity of the adsorbent surface induced by copper incorporation, which introduces adsorption sites with varying affinities. The relatively high surface area (~92 m²/g) and nanoscale particle size (~20.5 nm) contribute to the availability of diverse active sites. Additionally, 3D surface analysis indicated a moderate level of surface roughness (RMS ~7.5 nm), which supports the presence of sufficient accessible sites for interaction with dye molecules. These structural and morphological features collectively favour a multilayer adsorption mechanism, aligning well with the assumptions of the Freundlich model. Moreover, given the constant temperature conditions in this study, it is likely that the Temkin model, typically suited for temperature-dependent processes, exhibited lower compatibility compared to the Langmuir and Freundlich isotherms.

3.2.3. Adsorption kinetics

Understanding the adsorption mechanism requires a careful evaluation and comparison of various kinetic models. In this study, the adsorption kinetics of MB and RhB dyes onto Cu-doped TiO_2 NPs were investigated using pseudo-first-order, pseudo-second-order, intra-particle diffusion, and Elovich kinetic models. The experiments were carried out using an initial dye concentration of 5 ppm, and dye concentrations were monitored every 30 min using a UV-Vis spectrophotometer. Based on the measured concentrations (C_t), the adsorption capacity at time t (q_t) and other relevant parameters were calculated. The experimental data were then fitted to the selected kinetic models, and the corresponding parameters are presented in Table 6. As shown in Table 6, the Elovich model demonstrated the best fit for both dyes, with high correlation coefficients (R^2 = 0.9973 for MB and 0.9990 for RhB), indicating strong consistency with the experimental data. The superior performance of the Elovich model can likely be attributed to the adsorption behaviour and the physicochemical characteristics of the synthesized adsorbents. The kinetic data showed a rapid initial adsorption rate followed by a gradual decline, reaching equilibrium after approximately 90 min. This trend aligns well with the Elovich model, which describes chemisorption processes on heterogeneous surfaces. Copper doping in TiO_2 NPs introduces a variety of active sites with different energy levels and affinities, supported by their nanoscale size (~20.5 nm), relatively large specific surface area (~92 m²/g), and moderate surface roughness (~7.5 nm). These properties facilitate complex interactions between dye molecules and the adsorbent surface, including chemical bonding and site-specific adsorption. As the adsorption sites become progressively occupied, the rate of adsorption decreases due to increased surface coverage and activation energy barriers. The presence of copper ions likely enhances these chemisorptive interactions, which explains the time-dependent nature of the adsorption process. Accordingly, the Elovich model provides a more accurate representation of the observed kinetic behaviour compared to simpler models.

Table 6. Kinetic parameters for adsorption of dyes on Cu-doped TiO_2 NPs.

Kinetic models	Parameters	MB	RhB
Pseudo first order	R^2	0.9157	0.9179
	K_1 (min^{-1})	0.0491	0.0517
	q_e (mg/g)	17.9987	23.1686
Pseudo second order	R^2	0.9958	0.9975
	K_2 (g /(mg. min))	0.0041	0.0029
	q_e (mg/g)	11.8343	12.4223
Elovich	R^2	0.9973	0.9990
	α (mg /(g. min))	1.4506	2.2754
	β (g/mg)	0.4331	0.4845
Intra-particle diffusion	R^2	0.9562	0.9571
	K_i (mg /g. min $^{0.5}$)	0.6607	0.6472
	C (mg/g)	2.1119	2.6892

3.2.4. Comparison of adsorption performance with literature

To better evaluate the efficiency of the synthesized adsorbent, a comparison with previous studies was conducted. Table 7 lists several adsorbents reported in the literature along with their maximum adsorption capacities for dye pollutants in aqueous solutions. Among them, the Cu-doped TiO_2 adsorbent synthesized in the present study exhibited the highest adsorption capacity, reaching 19.0 mg/g for MB and 19.2 mg/g for RhB. This adsorbent was synthesized using a green synthesis method, which relies on non-toxic, environmentally friendly reagents and operates under mild conditions. Such an approach not

only minimizes environmental hazards but also reduces energy consumption and eliminates the need for hazardous waste disposal. Additionally, it lowers production costs and simplifies the separation process after water treatment, enhancing the overall economic feasibility.

Thus, the Cu-doped TiO_2 adsorbent developed in this study not only shows superior adsorption performance but also possesses excellent environmental and economic advantages, making its production and application highly valuable in the field of wastewater treatment.

Table 7. Comparison of different adsorbents for removal of dye pollutants.

Adsorbent	dye	Adsorption capacities, q_m, mg/g	Ref.
Fly ash	MB	1.88	Zhou *et al.*, 2025
Mg-modified fly ash	MB	14.34	Zhou *et al.*, 2025
CuS NPs	MB	15	Gupta *et al.*, 2012
Fe_3O_4 NPs	MB	10.47	Ramesh *et al.*, 2018
Activated carbon derived from Wheat Straw	MB	5.26	Benhadj *et al.*, 2023
Grape Pomace Biochar	MB	9.3	Kasemodel *et al.*, 2025
L-Asp capped Fe_3O_4 NPs	RhB	7.7	Belachew *et al.*, 2021
$CoFe_2O_4$	RhB	5.165	Oyetade *et al.*, 2015
Halloysite modified by ultrasound	RhB	8.37	Wierzbicka *et al.*, 2022
Halloysite modified by sulfuric acid	RhB	13.1	Wierzbicka *et al.*, 2022
Halloysite modified by resin	RhB	17.8	Wierzbicka *et al.*, 2022
Malachite NPs	Rhodamine 6G	8.40	Saikia *et al.*, 2013
TiO_2	Disperse Orange 30	11.44	Pankaj *et al.*, 2021
MgO	Orange G	18.1	Nassar *et al.*, 2017
Cone biomass	Reactive Red 195	7.38	Aksakal *et al.*, 2010
Rice Bran	Congo red	14.6	Wang *et al.*, 2009
Zeolite	Congo red	3.77	Vimonses *et al.*, 2009
Kaolin	Congo red	5.44	Vimonses *et al.*, 2009
Cu-doped TiO_2	MB	19	This study
Cu-doped TiO_2	RhB	19.12	This study

4. Conclusions

In this research, Cu-doped TiO_2 NPs with employing of Cannabis Sativa leaves were fabricated via green synthesis technique. Next, properties of NPs were appraised by XRD, FESEM, TEM, BET and EDAX analysis. Afterward, prepared NPs were applied in for removal of MB and RhB from the aqueous solution. Tests proved that the adsorbed amounts at 150 min were belong to the equilibrium data. Based on the obtained equilibrium data for each C_0 of each dye, q_t and other calculated parameters, matching of experimental data with various types of isotherm was done. It was revealed that among the Langmuir, Freundlich and Temkin adsorption isotherms, maximum R^2 was found for Freundlich isotherm. R^2 was 0.9979 and 0.9995 for MB and RhB, respectively. So, Freundlich isotherm described the adsorption process better than the other isotherms. Next, compatibility of experimental data with various adsorption kinetic models were tested. Applied models were as follow: pseudo first order, pseudo second order, Intra-particles diffusion and Elovich models. Among them, Elovich models by exhibiting the higher R^2 for both dyes exhibited the superior consistency by the experimental data. Maximum amount of R^2 for MB and RhB by employing of Elovich kinetic model were 0.9973 and 0.9990, respectively. Therefore, we can say that Freundlich isotherm and Elovich kinetic were very useful models for interpretation of MB and RhB adsorption on the Cu-doped TiO_2 NPs.

Author Contributions

Seyed Mehdi Sajjadi: Writing – original draft, Supervision, Project administration, Investigation, Data curation, Conceptualization.
Ghader Hosseinzadeh: Writing – review & editing, Validation, Methodology, software.

Conflict of Interest

The authors declare no financial or personal conflicts of interest that could influence the results reported in this manuscript.

Acknowledgements

The authors would like to express his deepest gratitude to University of Bonab, Bonab, Iran.

Data Availability Statement

All data used in the article are provided in the text and are available.

References

Abbasi, B. *et al.* (2018) 'Biogenic synthesis of Au, Ag and Au–Ag alloy nanoparticles using Cannabis sativa leaf extract', IET Nanobiotechnol., 12 (3), pp. 277-284. doi: https://doi.org/10.1049/iet-nbt.2017.0169

Abisharani, J. M. *et al.* (2020) 'Influence of 2,4-Diamino-6-Phenyl-1-3-5-triazine on bio synthesized TiO_2 dye-sensitized solar cell fabricated using poly (ethylene glycol) polymer electrolyte', Materials Research Express, 7 (2), p. 025507. doi: https://doi.org/10.1088/2053-1591/ab7066

Adamu, A., *et al.* (2023) 'Investigation of Cu/TiO_2 synthesis methods and conditions for CO_2 photocatalytic reduction via conversion of bicarbonate/carbonate to formate', Journal of CO_2 Utilization, 70, p. 102428. doi: https://doi.org/10.1016/j.jcou.2023.102428

Aguilar, T., *et al.* (2013) 'A route for the synthesis of Cu-doped TiO_2 nanoparticles with a very low band gap', *Chemical Physics Letters,* 571, pp. 49-53. doi: https://doi.org/10.1016/j.cplett.2013.04.007

Ahlawat, W., *et al.* (2020) 'Carbonaceous nanomaterials as effective and efficient platforms for removal of dyes from aqueous systems', *Environmental Research,* 181, p. 108904. doi: https://doi.org/10.1016/j.envres.2019.108904

Ahmad, M. M. *et al.* (2021) 'Investigation of TiO_2 Nanoparticles synthesized by sol-gel method for effectual photodegradation, Oxidation and Reduction Reaction', *Crystals*, 11(12). doi: https://doi.org/10.3390/cryst11121456.

Ahmad, N. *et al.* (2023) 'Insight into the adsorption thermodynamics, kinetics, and photocatalytic studies of polyaniline/SnS_2 nanocomposite for dye removal', *Journal of Hazardous Materials Advances,* 10, p. 100321. doi: https://doi.org/10.1016/j.hazadv.2023.100321

Aksakal, O. and Ucun, H. (2010) 'Equilibrium, kinetic and thermodynamic studies of the biosorption of textile dye (Reactive Red 195) onto Pinus sylvestris L', J*ournal of Hazardous Materials,* 181 (1), pp. 666-672. doi: https://doi.org/10.1016/j.jhazmat.2010.05.064

Al-Assaly, R. *et al.* (2024) 'Antimicrobial performance and instrumental analysis for hexagonal ZnO NPs biosynthesized via Ziziphus leaf extract', *Oxford Open Materials Science,* 4 (1), itae011. doi: https://doi.org/10.1093/oxfmat/itae011

An, B. (2020) 'Cu(II) and As(V) Adsorption Kinetic Characteristic of the Multifunctional Amino Groups in Chitosan', *Processes*, 8(9), p. 1194. doi: https://doi.org/10.3390/pr8091194.

Baratta, M., Nicoletta, F. P. and De Filpo, G. (2025) 'Graphene Oxide-Doped CNT Membrane for Dye Adsorption', *Nanomaterials,* 15 (11), p. 782. doi: https://doi.org/doi:10.3390/nano15110782

Belachew, N., *et al.* (2021) 'Synthesis of amino acid functionalized Fe_3O_4 nanoparticles for adsorptive removal of Rhodamine B', *Applied Water Science,* 11, p. 33. doi: https://doi.org/10.1007/s13201-021-01371-y

Benhadj, M., *et al.* (2023) 'Wheat Straw-Derived Activated Carbon for Efficient Removal of Methylene blue: Kinetics, Thermodynamics, and Adsorption Mechanism', *Key Engineering Materials,* 954, pp. 73-93. doi: https://doi.org/10.4028/p-6CKBMf

BinSabt, M., *et al.* (2022) 'Green Synthesis of CS-TiO_2 NPs for efficient photocatalytic degradation of methylene blue dye', *Polymers,* 14 (13), p. 2677. doi: https://doi.org/10.3390/polym14132677

Bopape, D. A., Ntsendwana, B. and Mabasa, F. D. (2024) 'Photocatalysis as a pre-discharge treatment to improve the effect of textile dyes on human health: A critical review', *Heliyon,* 10 (20), p. e39316. doi: https://doi.org/10.1016/j.heliyon.2024.e39316

Cheng, H., *et al.* (2014) 'Effect of phase composition, morphology, and specific surface area on the photocatalytic activity of TiO_2 nanomaterials', *RSC Advances,* 4 (87), pp. 47031-47038. doi: https://doi.org/10.1039/C4RA05509H

Cheung, C. W., Porter, J. F. and McKay, G. (2000) 'Elovich equation and modified second-order equation for sorption of cadmium ions onto bone char', *Journal of Chemical Technology & Biotechnology,* 75 (11), pp. 963-970. Available at: https://doi.org/10.1002/1097-4660(200011)75:11%3C963::AID-JCTB302%3E3.0.CO;2-Z (Acccessed date: 21 May 2025).

Chiani, E., *et al.* (2020) 'Adsorption of cationic dye from aqueous solution using SBA-15 nano particles synthesized by stem sweep ash as the source of silica', *Journal of Applied Research in Water and Wastewater,* 7 (2), pp. 172-179. doi: https://doi.org/10.22126/arww.2021.5648.1186

Chu, K. H. (2021) 'Revisiting the Temkin Isotherm: Dimensional inconsistency and approximate forms', *Industrial & Engineering Chemistry Research,* 60 (35), pp. 13140-13147. doi: https://doi.org/10.1021/acs.iecr.1c01788

Csakvari, A. C., *et al.* (2021) 'Green synthesis, characterization, and antibacterial properties of silver nanoparticles obtained by using diverse varieties of cannabis sativa leaf extracts', *Molecules,* 26 (13), p. 4041. doi: https://doi.org/doi:10.3390/molecules26134041

Dada, A. O. *et al.* (2012) 'Langmuir, Freundlich, Temkin and Dubinin–Radushkevich isotherms studies of equilibrium sorption of Zn^{2+} unto phosphoric acid modified rice husk', *IOSR Journal of Applied Chemistry,* 3 (1), pp. 38-45. doi: https://doi.org/10.9790/5736-0313845.

Deliza, D. *et al.* (2025) 'Green synthesis approach on fabrication of TiO_2 nanoparticle using peel extract of Baccaurea racemosa for photocatalytic degradation of Acid Red-185', *Environmental Nanotechnology, Monitoring & Management,* 23, p. 101074. doi: https://doi.org/10.1016/j.enmm.2025.101074

Dutta, S. *et al.* (2024) 'Contamination of textile dyes in aquatic environment: Adverse impacts on aquatic ecosystem and human health, and its management using bioremediation', *Journal of Environmental Management,* 353, p. 120103. doi: https://doi.org/10.1016/j.jenvman.2024.120103

Eddy, D. R. *et al.* (2024) 'A review of recent developments in green synthesis of TiO_2 nanoparticles using plant extract: Synthesis, characterization and photocatalytic activity', *Inorganic Chemistry Communications,* 165, p. 112531. doi: https://doi.org/10.1016/j.inoche.2024.112531

Gadge, A. S. *et al.* (2025) 'Novel green synthesis of Gd-doped TiO_2 nanoparticles for environmental remediation: statistical modeling and process optimization', *New Journal of Chemistry,* 49 (14), pp. 5995-6011. doi: https://doi.org/10.1039/D5NJ00856E

Gupta, V. K. *et al.* (2012) 'Adsorptional photocatalytic degradation of methylene blue onto pectin–CuS nanocomposite under solar light', *Journal of Hazardous Materials,* 243, pp. 179-186. doi: https://doi.org/10.1016/j.jhazmat.2012.10.018

Habeeb, S. A., Zinatizadeh, A. A. and Zangeneh, H. (2023) 'Photocatalytic Decolorization of Direct Red16 from an Aqueous Solution Using B-ZnO/TiO_2 Nano Photocatalyst: Synthesis, Characterization, Process Modeling, and Optimization', *Water,* 15 (6), p. 1203. doi: https://doi.org/10.3390/w15061203

Ho, D. Q. *et al.* (2025) 'Green Synthesis of TiO_2-CeO_2 nanocomposites using plant extracts for efficient organic dye photodegradation', *Catalysts,* 15 (6), p. 583. doi: https://doi.org/10.3390/catal15060583

Hosseinzadeh, G. *et al.* (2024) 'Construction of PVC/PVA WO_3 3D nanostructure thin film nanocomposite for treatment of oil refinery wastewater', *Journal of Polymers and the Environment,* 32, pp. 1879-1891. doi: https://doi.org/10.1007/s10924-023-03077-5

Jadhav, V. *et al.* (2025) 'Green synthesis of Ag@TiO_2 nanomaterials using Achyranthes aspera leaf extract for sustainable photocatalytic degradation of dyes', *Discover Applied Sciences,* 7 (7), pp. 732. doi: https://doi.org/10.1007/s42452-025-07324-3

Jaramillo-Fierro, X. and Cuenca, G. (2024) 'Enhancing Methylene Blue Removal through Adsorption and Photocatalysis—A Study on the GO/$ZnTiO_3$/TiO_2 Composite', *International Journal of Molecular Sciences,* 25 (8), p. 4367. doi: https://doi.org/10.3390/ijms25084367

Jayapriya, M. and Arulmozhi, M. (2021) 'Beta vulgaris peel extract mediated synthesis of Ag/TiO_2 nanocomposite: Characterization, evaluation of antibacterial and catalytic degradation of textile dyes-an electron relay effect', *Inorganic Chemistry Communications,* 128, p. 108529. doi: https://doi.org/10.1016/j.inoche.2021.108529

Kasemodel, M. C. *et al.* (2025) 'The Investigation of the Adsorption of Methylene Blue from Water by Torrefied Biomass', *Colorants,* 4 (2), p. 21. doi: https://doi.org/10.3390/colorants4020021

Khan, M. A. M. *et al.* (2022) 'Characterization and photocatalytic performance of hydrothermally synthesized Cu-doped TiO_2 NPs', *Optical Materials,* 133, p. 112983. doi: https://doi.org/10.1016/j.optmat.2022.112983

Khin, M. M. *et al.* (2012) 'A review on nanomaterials for environmental remediation', *Energy & Environmental Science,* 5 (8), pp. 8075-8109. doi: https://doi.org/10.1039/C2EE21818F

Kuvarega, A. T. and Mamba, B. B. (2017) 'TiO_2-based photocatalysis: toward visible light-responsive photocatalysts through doping and fabrication of carbon-based nanocomposites', *Critical Reviews in Solid State and Materials Sciences,* 42 (4), pp. 295-346. doi: https://doi.org/10.1080/10408436.2016.1211507

MiarAlipour, S. *et al.* (2018) 'TiO_2/porous adsorbents: Recent advances and novel applications', *Journal of Hazardous Materials,* 341, pp. 404-423. doi: https://doi.org/10.1016/j.jhazmat.2017.07.070

Molla, A., *et al.* (2019) 'Selective adsorption of organic dyes on graphene oxide: Theoretical and experimental analysis', *Applied Surface Science,* 464, pp. 170-177. doi: https://doi.org/10.1016/j.apsusc.2018.09.056

Munyegaju, J. *et al.* (2022) 'Textile effluent treatment using Avocado seeds based activated carbon', *Journal of Applied Research in Water and Wastewater,* 9 (1), pp. 83-90. doi: https://doi.org/10.22126/arww.2022.8008.1258

Nabi, G., *et al.* (2021) 'Green synthesis of spherical TiO_2 nanoparticles using Citrus Limetta extract: Excellent photocatalytic water decontamination agent for RhB dye', *Inorganic Chemistry Communications,* 129, p. 108618. doi: https://doi.org/10.1016/j.inoche.2021.108618

Nagaraj, G. *et al.* (2021) 'Effects of the surface of solar-light photocatalytic activity of Ag-doped TiO_2 nanohybrid material prepared with a novel approach', *Applied Physics A,* 127, p. 269. doi: https://doi.org/10.1007/s00339-021-04427-7

Nassar, M. Y. *et al.* (2017) 'MgO nanostructure via a sol-gel combustion synthesis method using different fuels: An efficient nano-adsorbent for the removal of some anionic textile dyes', *Journal of Molecular Liquids,* 225, pp. 730-740. doi: https://doi.org/10.1016/j.molliq.2016.10.135

Natsir, M., *et al.* (2021) 'Synthesis and charcterization of Cu-doped TiO_2 (Cu/TiO_2) nanoparticle as antifungal phytophthora palmivora', *Journal of Physics: Conference Series,* 1899 (1), p. 012039. doi: https://doi.org/10.1088/1742-6596/1899/1/012039

Nawaz, A. *et al.* (2023) 'Solar light driven degradation of textile dye contaminants for wastewater treatment - studies of novel polycationic selenide photocatalyst and process optimization by response surface methodology desirability factor', *Chemosphere,* 328, p. 138476. doi: https://doi.org/10.1016/j.chemosphere.2023.138476

Nayebzadeh, H., Naderi, F. and Rahmanivahid, B. (2021) 'Effect of doping Al cations into $MgFe_2O_4$ magnetic structure for efficient removals of methyl orange dye from water', *Journal of Inorganic and Organometallic Polymers and Materials,* 31 (2), pp. 776-789. doi: https://doi.org/10.1007/s10904-020-01816-y

Osmari, T. A. *et al.* (2013) 'Statistical analysis of linear and non-linear regression for the estimation of adsorption isotherm parameters', *Adsorption Science & Technology,* 31 (5), pp. 433-458. doi: https://doi.org/10.1260/0263-6174.31.5.433

Oyetade, O. A. *et al.* (2015) 'Effectiveness of carbon nanotube–cobalt ferrite nanocomposites for the adsorption of rhodamine B from aqueous solutions', *RSC Advances,* 5 (29), pp. 22724-22739. doi: https://doi.org/10.1039/C4RA15446K

Pankaj, Sharma, R. and Verma, S. K. (2021) 'Equilibrium, kinetic and mechanism studies on adsorption of textile disperse dye from aqueous solution onto TiO_2 in the presence of ultrasound and rare earth ions', *Materials Today: Proceedings,* 44, pp. 2158-2167. doi: https://doi.org/10.1016/j.matpr.2020.12.279

Piaskowski, K., Świderska-Dąbrowska, R. and Zarzycki, P. K. (2019) 'Dye removal from water and wastewater using various physical, chemical, and biological processes', *Journal of AOAC INTERNATIONAL,* 101 (5), pp. 1371-1384. doi: https://doi.org/10.5740/jaoacint.18-0051

Rahmanivahid, B., Naderi, F. and Nayebzadeh, H. (2020) 'Removing methyl orange molecules from aqueous medium by magnetic nanoparticles: Evaluating adsorption factors, isotherms, kinetics and thermodynamics', *Journal of Water and Environmental Nanotechnology,* 5 (1), pp. 1-16. doi: https://doi.org/10.22090/jwent.2020.01.001

Ramesh, A. V. *et al.* (2018) 'Facile green synthesis of Fe_3O_4 nanoparticles using aqueous leaf extract of Zanthoxylum armatum DC. for efficient adsorption of methylene blue', *Journal of Asian Ceramic Societies,* 6 (2), pp. 145-155. doi: https://doi.org/10.1080/21870764.2018.1459335

Ramzan, M. *et al.* (2021) 'Green synthesis of Cu@TiO_2 via cedrus deodara leaf extract: A novel composite with high photocatalytic and antibacterial activity', *Current Research in Green and Sustainable Chemistry,* 4, p. 100137. doi: https://doi.org/10.1016/j.crgsc.2021.100137

Revellame, E. D. *et al.* (2020) 'Adsorption kinetic modeling using pseudo-first order and pseudo-second order rate laws: A review', *Cleaner Engineering and Technology,* 1, p. 100032. doi: https://doi.org/10.1016/j.clet.2020.100032

Sadeghpour, P. *et al.* (2022) 'Ultrasonic-promoted growth of staggered heterostructured tin(II) oxide nanoparticles on bulk carbon nitride nanolayer: Activated in solar spectrum with enhanced photocatalytic treatment of dyes effluents', *Solar Energy,* 241, pp. 437-451. doi: https://doi.org/10.1016/j.solener.2022.06.027

Saikia, J. *et al.* (2013) 'Malachite nanoparticle: A potent surface for the adsorption of xanthene dyes', *Journal of Environmental Chemical Engineering,* 1 (4), pp. 1166-1173. doi: https://doi.org/10.1016/j.jece.2013.09.002

Saini, R. and Kumar, P. (2023) 'Green synthesis of TiO_2 nanoparticles using Tinospora cordifolia plant extract & its potential application for photocatalysis and antibacterial activity', *Inorganic Chemistry Communications,* 156, p. 111221. doi: https://doi.org/10.1016/j.inoche.2023.111221

Sajjadi, S. M. (2024) 'Evaluation of the various adsorption isotherm models for the photocatalytic removal of methylene blue from the wastewater by graphene oxide/TiO_2/SiO_2', *Journal of Applied Research in Water and Wastewater,* 11 (1), pp. 59-66. doi: https://doi.org/10.22126/arww.2023.8980.1286

Sajjadi, S. M. and Etemadi, H. (2025a) 'Effect of Ni/Al_2O_3 nanoparticles on the antifouling properties of polyvinyl chloride membranes in water treatment', *International Journal of Environmental Science and Technology,* 22 (10), pp. 9157-9174. doi: https://doi.org/10.1007/s13762-025-06451-z

Sajjadi, S. M., Etemadi, H. and Zaremanesh, M. (2024a) 'Synthesis and evaluation of PVC-Cu/Al_2O_3 nanocomposite membranes for removing of natural organic matter from the wastewater', *Asia-Pacific Journal of Chemical Engineering,* 19 (4), p. e3082. doi: https://doi.org/10.1002/apj.3082

Sajjadi, S. M., Fardi Ilkhchy, A. and Aygani, A. (2025b) 'Investigating the efficiency of the ultrasonic-assisted sol-gel synthesized Cu/ZnO photocatalysts in degradation of textile dyes', *Materials Chemistry and Physics,* 337, p. 130590. doi: https://doi.org/10.1016/j.matchemphys.2025.130590

Sajjadi, S. M., Haghighi, M. and Eshghi, J. (2019) 'Synergic influence of potassium loading and plasma-treatment on anti-coke property of K-Promoted bimetallic NiCoNiAl_2O_4 nanocatalyst applied in O_2-Enhanced dry reforming of CH_4', *International Journal of Hydrogen Energy,* 44 (26), pp. 13397-13414. doi: https://doi.org/10.1016/j.ijhydene.2019.03.260

Sajjadi, S. M. *et al.* (2022a) 'Various calcium loading and plasma-treatment leading to controlled surface segregation of high coke-resistant Ca-promoted NiCo–NiAl_2O_4 nanocatalysts employed in CH_4/CO_2/O_2 reforming to H_2', I*nternational Journal of Hydrogen Energy,* 47 (59), pp. 24708-24727. doi: https://doi.org/10.1016/j.ijhydene.2022.05.233

Sajjadi, S. M., Haghighi, M. and Rahmani, F. (2022b) 'On the synergic effect of various anti-coke materials (Ca–K–W) and glow discharge plasma on Ni-based spinel nanocatalyst design for syngas production via hybrid CO_2/O_2 reforming of methane', J*ournal of Natural Gas Science and Engineering,* 108, p. 104810. doi: https://doi.org/10.1016/j.jngse.2022.104810

Sajjadi, S. M. and Hosseinzadeh, G. (2025c) 'Utilization of green synthesized calcium doped TiO_2 photocatalysts for the solar-light-driven degradation of dyes in aqueous solution', *Journal of Nanostructures,* 15 (2), pp. 684-701. doi: https://doi.org/10.22052/jns.2025.02.027

Sajjadi, S. M. and Hossinzadeh, G. (2024b) 'Textile dyes removing from the wastewater by green synthesized Cu-doped ZnO photocatalysts under the simulated sunlight illumination', *Ceramics International, 50 (19, Part B)*, pp. 36271-36285. doi: https://doi.org/10.1016/j.ceramint.2024.07.011

Shahzadi, T. *et al.* (2022) 'Eco-friendly synthesis of ZnO nanoparticles using Cannabis sativa and assessment of its activities as efficient dyes removal and antioxidant agent', *International Journal of Environmental Analytical Chemistry,* 102 (16), pp. 4738-4756. doi: https://doi.org/10.1080/03067319.2020.1789610

Sharma, J. *et al.* (2022) 'Toxic effects of Rhodamine B on antioxidant system and photosynthesis of Hydrilla verticillata', *Journal of Hazardous Materials Letters,* 3, pp. 100069. doi: https://doi.org/10.1016/j.hazl.2022.100069

Verma, V., *et al.* (2022) 'A Review on green synthesis of TiO_2 NPs: Photocatalysis and antimicrobial applications', *Polymers,* 14 (7), p. 1444. doi: https://doi.org/doi:10.3390/polym14071444

Vieira, G. B. *et al.* (2018) 'CeO_2/TiO_2 nanostructures enhance adsorption and photocatalytic degradation of organic compounds in aqueous suspension', *Journal of Photochemistry and Photobiology A: Chemistry,* 353, pp. 325-336. doi: https://doi.org/10.1016/j.jphotochem.2017.11.045

Vimonses, V. *et al.* (2009) 'Kinetic study and equilibrium isotherm analysis of Congo Red adsorption by clay materials', *Chemical Engineering Journal,* 148 (2), pp. 354-364. doi: https://doi.org/10.1016/j.cej.2008.09.009

Wang, X. S. and Chen, J. P. (2009) 'Biosorption of Congo Red from aqueous solution using wheat bran and rice bran: batch studies', *Separation Science and Technology,* 44 (6), pp. 1452-1466. doi: https://doi.org/10.1080/01496390902766132

Wierzbicka, E. *et al.* (2022) 'Efficient Rhodamine B dye removal from water by acid- and organo-modified halloysites', *Minerals,* 12 (3), p. 350. doi: https://doi.org/10.3390/min12030350

Yitagesu, G. B., Leku, D. T. and Workneh, G. A. (2023) 'Green synthesis of TiO_2 using impatiens rothii hook.f. leaf extract for efficient removal of methylene blue dye', *ACS Omega,* 8 (46), pp. 43999-44012. doi: https://doi.org/10.1021/acsomega.3c06142

Zhou, J. *et al.* (2025) 'Study on the adsorption characteristics of methylene blue by magnesium-modified fly ash', *Molecules,* 30 (5), p. 992. doi: https://doi.org/10.3390/molecules30050992